Dynamics of fractures in quenched disordered media

Guido Caldarelli,[1,2] Raffaele Cafiero,[3,4] and Andrea Gabrielli[4,5]
[1]*Theory of Condensed Matter, Cavendish Laboratory Madingley Road, CB3 0HE Cambridge, United Kingdom*
[2]*Department of Theoretical Physics, The University, M13 9PL Manchester, United Kingdom*
[3]*Max-Planck Institute for Physics of Complex Systems, Nöhnitzer Strasse 38, 01187 Dresden, Germany*
[4]*INFM–Unità di Roma I, Università di Roma ''La Sapienza,'' Piazzale Aldo Moro 2, I-00185 Roma, Italy*
[5]*Dipartimento di Fisica, Università di Roma ''Tor Vergata,'' via della Ricerca Scientifica 1, 00133 Roma, Italy*
(Received 20 October 1997)

We introduce a model for fractures in quenched disordered media. This model has a deterministic extremal dynamics, driven by the energy function of a network of springs (Born Hamiltonian). The breakdown is the result of the cooperation between the external field and the quenched disorder. This model can be considered as describing the low-temperature limit for crack propagation in solids. To describe the memory effects in this dynamics and then to study the resistance properties of the system we realized some numerical simulations of the model. The model exhibits interesting geometric and dynamical properties, with a *strong reduction* of the fractal dimension of the clusters and of their backbone, with respect to the case in which thermal fluctuations dominate. This result can be explained by a recently introduced theoretical tool as a *screening enhancement* due to memory effects induced by the quenched disorder. [S1063-651X(98)03604-6]

PACS number(s): 05.40.+j, 02.50.−r, 62.20.Mk

I. INTRODUCTION

In recent years, many models have been proposed to describe the formation of cracks in different kind of materials [1–4]. They are inspired by the study of nonequilibrium fractal growth processes such as the dielectric breakdown model (DBM) [5] and diffusion-limited aggregation [6]. These models are based on two different mechanisms for the fracture growth: (i) a *stochastic* effect due to the thermal fluctuations in the medium, driven by an external field, and (ii) a *deterministic* dynamics, when the main source of randomness is the quenched disorder of the medium [like in the invasion percolation (IP) model [7]], the thermal fluctuations being negligible (i.e., low-temperature limit).

A very interesting model, belonging to the first class, is the Born model (BM) [8,9], where minimization of the elastic energy is used to compute the driving field. This model for fracture propagation is the analog of the DBM for Laplacian growth. It describes the fracture's propagation as a stochastic process, where the probabilistic mechanism represents growth instabilities, like, for example, density fluctuations in a gas. In this approach the quenched disorder of the medium is negligible.

In this paper we want to consider the limit of low temperature for the BM, where the driving field cooperates with quenched disorder to produce the breakdown patterns. The quenched disorder can be thought to represent the effect, at a mesoscopic scale, of defects of the breaking layer. In this version of the model, at each time step the growing bond is selected deterministically, i.e., the bond with the smallest ratio between the local driving field and the quenched disorder grows. The system is a two-dimensional triangular lattice of springs. We apply to two parallel boundaries of the system a uniaxial tension and fixed boundary condition to the others. In this way we obtain directed, crack patterns, orthogonal to the applied stress. The system has two independent length scales: the height h and the width L. This allows us to evaluate more clearly the various scaling regimes of these structures. Usually, with this boundary condition, two different phases, called, respectively, the *scaling regime* and *steady state*, are present [10].

We will see that in the quenched version of the BM (QBM), because of the very strong screening on the growth process, the first regime (where many different branches compete during the growth) is nearly absent. In fact, most of the growth dynamics develops during the steady state, where only one branch survives and the cluster is statistically self-similar with well-defined fractal properties. Together with the fractal dimension, the backbone and chemical distance exponents characterize completely the fractures produced by our model.

We compare our results with those obtained previously for the stochastic version of the BM [9], showing that the fractal dimension of the clusters and of the backbone, in similar conditions, are *strongly reduced*. We explain this as a consequence of the absence of thermal fluctuations; the quenched disorder produces *memory effects* giving screening effects similar to those of IP [12]. On the other hand, in the same conditions, the screening effect produced by the modulation of the driving field gives a fractal dimension much smaller than the IP, which is the limit of the model in which there is no external driving field or it is constant. The same qualitative result has been found recently, both numerically and analytically, for the quenched version of the DBM [13]. Therefore, the numerical results found here for the QBM support the belief that this screening enhancement is a general property of all deterministic models with quenched disorder and a driving field.

The distribution of the quenched disorder related to the grown (broken) sites (acceptance profile) is also studied for different values of the model parameters. This distribution reaches, during the evolution, an asymptotic shape. In the case of IP, the asymptotic distribution is a step function, with the discontinuity at the value of quenched disorder coinci-

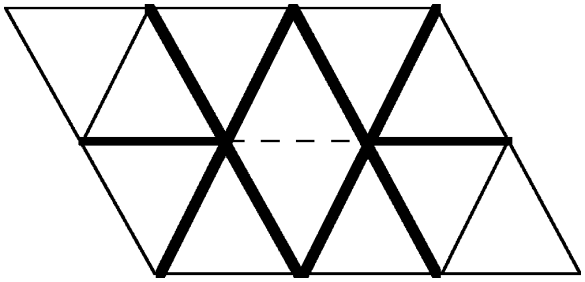

FIG. 1. Connectivity condition. Broken bonds are indicated by dashed lines, while interface bonds are indicated by thick lines.

dent with the critical point of classic percolation [7,14]. This steplike shape of the acceptation profile indicates that the dynamics develops avalanches with a scale-invariant distribution [11,12].

In our model, the presence of the stress field, however, does not allow the presence of a critical threshold in this asymptotic distribution of quenched disorder. As a consequence, the dynamics does not develop scale-invariant avalanches, but these avalanches have a typical size [12,13]. A very important universality relation can be written, which explains, in terms of the dependence of the fractal properties on the parameters of the model, the cooperation between the driving field and the quenched disorder in developing such a fractal structure.

The paper is organized as follows. In Sec. II the model is introduced and compared with the corresponding stochastic model. The details for the realization of simulations are specified. In Sec. III we describe our numerical results for the fractal properties of the clusters, the backbone, and the chemical distance, for the roughness exponent of the chemical distance, and for the statistical effective distribution of quenched variables on the growth interface. In Sec. IV the universality relation is demonstrated and a theoretical tool is introduced to explain the two screening effects in producing fractal properties. Finally, in Sec. V we discuss the results and draw some conclusions.

II. MODEL

The BM describes the medium as a discrete set of springs. The equilibrium state is obtained by imposing minimization of the energy, while dynamics of fracture is given by assigning a rule of growth. Concerning the equilibrium state, we imagine breaking only one spring at a time to model a system of slowly developing fractures and after every breakdown a new equilibrium state is computed. We describe the energy of the system by means of the same potential energy. This elastic potential energy consists of two different terms, describing, respectively, a central force and a noncentral force contribution:

$$V=\frac{1}{2}\sum_{i,j} V_{i,j}=\frac{1}{2}\sum_{i,j} (\alpha-\beta)[(\vec{u}_i-\vec{u}_j)\cdot\hat{r}_{i,j}]^2+\beta[\vec{u}_i-\vec{u}_j]^2, \tag{1}$$

where $\vec{u}_i$ is the displacement vector for site i, $\hat{r}_{i,j}$ is the unity vector between i and j, α and β are force constants, and the sum is over the nearest-neighbor sites connected by an unbroken spring.

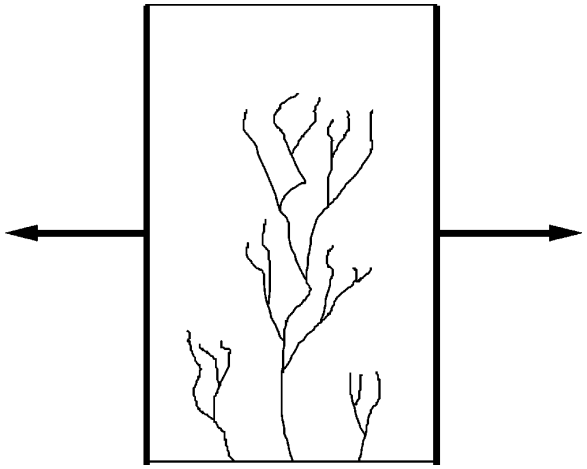

FIG. 2. Uniaxial tension applied to the lattice.

For any equilibrium state $\vec{\nabla}_{\{\vec{u}_i\}}V(\vec{u}_i,\vec{u}_j)=0\ \forall i$ must result where j is the nearest neighbor of i. This condition yields a series of equations for the $\vec{u}_i$'s that can be solved by imposing the boundary condition. The initial boundary condition is a uniform dilation on the left- and right-hand sides of the sample. This boundary condition changes, taking into account all the springs broken during the evolution of the crack.

Concerning the rule of growth, we have chosen a deterministic rule selecting the bond to break according to its ''generalized elongation'' $V_{i,j}^{1/2}$. The particular rule explained in the following equations has been inspired by analogies with the DBM. We think of $V_{i,j}^{1/2}$ as a field acting on the spring between sites i and j. Since the system is characterized by the presence of random quenched defects (represented as a quenched random noise), we assign to each spring a random number $x_{i,j}$ extracted by the probability density

$$p_0(x_{i,j})=\frac{a}{x_{sup}^a}x_{i,j}^{a-1}, \tag{2}$$

where the parameter a $(a\in[0,\infty))$ modulates the importance of the disorder in the mechanical properties of the system and the variables are defined in the range $[0,x_{sup}]$. From Eq. (2) one can derive the mean value $\langle x\rangle$ of the disorder assigned to the bonds:

$$\langle x\rangle=\int_0^{x_{sup}} dx\ x\ p_0(x)=\frac{a}{a+1}x_{sup}. \tag{3}$$

A ''fragile'' material corresponds to small values of a ($\langle x\rangle \simeq 0$), while a ''rigid'' one corresponds to big values of a ($\langle x\rangle \simeq x_{sup}$). Then we define a set of dynamical variables

$$y_{i,j}(t)=A_{i,j}(t)x_{i,j}, \tag{4}$$

where $A_{i,j}(t)=1/V_{i,j}(t)^{1/2}$. Then, at each time step, the spring with the smallest value $y_{i,j}(t)$ on the growth interface of the fracture is broken.

It is customary to modulate the influence of the stress field on the growth dynamics with the introduction of a parameter

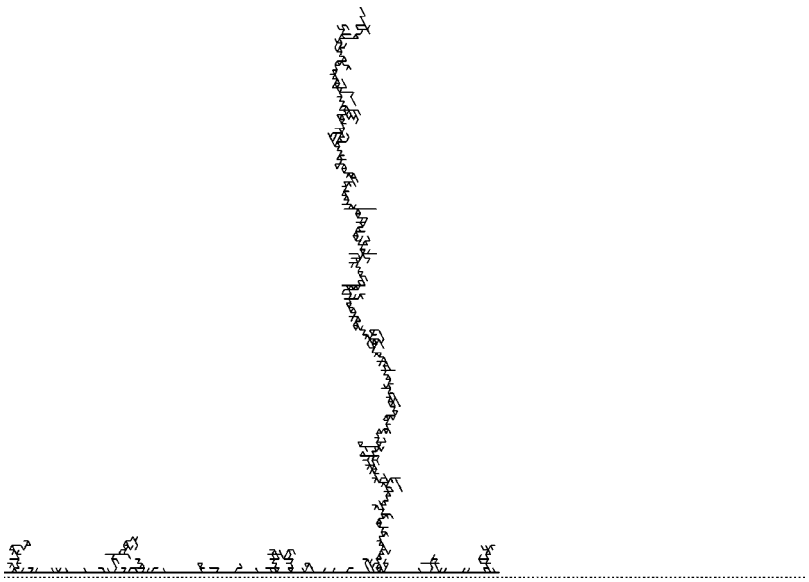

FIG. 3. Crack pattern generated by our model, with the parameters $\eta=1.0$, $a=1.0$, $\alpha=1.0$, and $\beta=0.5$.

η. In this case the formula for $A_{i,j}$ becomes $A_{i,j}(t)=1/V_{i,j}(t)^{\eta/2}$. When $\eta=0$ there is no field and the model has the same dynamics as invasion percolation [13], while $\eta=\infty$ corresponds to an infinite strength of the field and the cluster is a one-dimensional straight line. In fact, the disorder effects are negligible when compared to an infinite field. Some details have to be specified since, in principle, their variation could affect the fractal properties [8,15,16]. Due to the vectorial nature of Eq. (1) a triangular lattice is more appropriate to model the medium. In fact, for a squared lattice when $\beta=0$, the system behaves as a set of independent planes without a connection between each other. For this reason we will follow [9,17], by considering only triangular lattices. Furthermore, the growth interface at any time is given by the set of unbroken bonds that are nearest neighbors to the cluster of broken bonds (i.e., the perimeter of the fracture cluster). This corresponds to the implementation of a connectivity condition (Fig. 1).

III. NUMERICAL SIMULATIONS

We performed several realizations on systems of size $L\times L$ $(L=64,128)$, in triangular geometry (with periodic boundary conditions on the top and bottom). A quenched variable $x_{i,j}$ is assigned to each bond i,j. The $x_{i,j}$'s follow the distribution function of Eq. (2) with $x_{sup}=0.5$. In fact, a constant strain equal to 0.5 lattice units is applied in the horizontal direction (see Fig. 2). At each time step, the stress field over the interface bonds is computed. Then the bond with the smallest value $y_{i,j}$ is broken, the new stress fields are computed, and new bonds are added to the perimeter. By iterating this dynamics, one obtains structures such as that shown in Fig. 3.

The most important quantity characterizing the structures generated by the model is the fractal dimension D_f. For each value of L, we have generated a set of 20 realizations and computed the fractal dimension by the box-counting method. This has been done for different values of β/α. In fact, in the equilibrium condition $\vec{\nabla}_{\{\vec{u}_i\}}V(\vec{u}_i)=0$ we deal only with the ratio β/α. For this reason, we decided to vary β and keep $\alpha=1$. Furthermore, we performed the same analysis also by varying η (the parameter modulating the effects of the field) and a (the parameter modulating the disorder). Our results are shown in Tables I–III.

The model shows a continuous dependence of the fractal dimension on the parameter β, as found in [9] for the stochastic BM. The dependence of the fractal dimension on the parameters η and a is different and interesting. In fact, from our simulations we see that the fractal dimension actually *depends only on the product* $a\eta$. This introduces a precise relationship between the indices describing the properties of the medium and the properties of the stress field.

If we compare this result with the case of invasion percolation, where the field is absent and the fractal dimension does not depend on the value of a [7,12], we see that the introduction of the stress field breaks the symmetry with respect to a, leading to less universal ''critical'' properties. In Sec. IV we present an analytical demonstration of this universal property.

TABLE I. Behavior of the fractal dimension of the QBM for different values of β, with $a=1$ and $\eta=1$, for sizes $L=64,128$.

β	D_f $(L=64)$	D_f $(L=128)$
0.0	1.15 ± 0.03	1.14 ± 0.02
0.005	1.18 ± 0.03	1.16 ± 0.02
0.05	1.20 ± 0.03	1.17 ± 0.02
0.5	1.22 ± 0.02	1.20 ± 0.02
5	1.26 ± 0.02	1.24 ± 0.02

TABLE II. Fractal dimension of the QBM for different values of η and a for clusters of size $L=64$. The values of the other parameters are $\beta=0.5$ and $\alpha=1$.

η	D_f $(\eta,a=1)$	a	D_f $(\eta=1,a)$
0.5	1.36 ± 0.03	0.5	1.33 ± 0.03
1.0	1.21 ± 0.03	1.0	1.21 ± 0.03
2.0	1.13 ± 0.03	2.0	1.15 ± 0.03
3.0	1.10 ± 0.03	3.0	1.10 ± 0.03

TABLE III. Fractal dimension of the QBM for different values of η and a for clusters of size $L=128$. The values of the other parameters are $\beta=0.5$ and $\alpha=1$.

η	$D_f(\eta,a=1)$	a	$D_f(\eta=1,a)$
0.5	1.42 ± 0.02	0.5	1.40 ± 0.02
1.0	1.20 ± 0.02	1.0	1.20 ± 0.02
2.0	1.15 ± 0.02	2.0	1.16 ± 0.02
3.0	1.11 ± 0.02	3.0	1.10 ± 0.02

As it can be noted, for fixed a, the fractal dimension of the fracture cluster, for any value of $\eta>0$, is less than the IP one. This is due to the fact that for $\eta>0$, there is a screening effect related to the physical stress field, in addition to the screening related to the memory effects of the quenched disorder. Moreover, our numerical results show clearly that in a fragile material (small a, $\langle x\rangle\simeq 0$) the fractures have a big fractal dimension, while in a rigid material (big a, $\langle x\rangle \simeq x_{sup}$) the fractures tend to be straight lines with fractal dimension near 1. This result sounds qualitatively reasonable from an experimental point of view. A fragile material could correspond to a material with many impurities that lower its resistance to rupture, allowing many bonds to be broken. A rigid material could represent a material without impurities at zero temperature, in which fractures are straight lines along the direction of maximum stress. However, a quantitative comparison with experiments is still not accessible since it needs a clear connection between what we call quenched disorder in our model, which we believe to give a description of the system at a mesoscopic scale, and the microscopic disorder in real systems.

In Sec. IV we will propose an analytical explanation for our numerical findings. The same qualitative results have been found recently for a similar model: the quenched dielectric breakdown model (QDBM) [13]. This suggests that the dependence on the product of a and η of the dynamics and the geometry of the patterns plus a *screening enhancement* effect are general properties of all the deterministic models with the driving field in the presence of quenched disorder.

A further characterization of the topological and connectivity properties of the aggregates is given by the exponents ruling the scaling of two subsets of the clusters: the chemical distance and the backbone. The chemical distance is the shortest path between the two ends of the aggregate and shows interesting self-affine properties. The backbone is obtained by cutting from the cluster all the tips and the dangling loops connected to the chemical distance (see Fig. 4). This part of the cluster influences the macroscopic transport properties of the medium, while the chemical distance gives the shape of the line separating the system into two parts after the breakdown. It is worth pointing out that in models with a scalar external field, such as the DBM [5] and QDBM [13], no closed loops are allowed and the backbone trivially coincides with the chemical distance [9].

To determine the backbone and the chemical distance we followed a method used in [9], based on the topological properties of the clusters. As an example, in Figs. 5 and 6 we show, respectively, the backbone and the chemical distance we obtain for the cluster of Fig. 3. In Table IV we collect the results of a box-counting analysis. The backbone fractal dimension is significantly larger than one, although quite smaller than for the stochastic Born model [9]. Instead, the fractal dimension of the chemical distance is 1 for both $L=64$ and $L=128$.

We then studied the roughness exponent χ of the chemical distance, which gives the scaling of the mean-squared lateral width $W(l)$ of a self-affine path with respect to its length l [18]. In our case, the path develops vertically and its length is measured along the vertical direction, while the width is computed along the horizontal direction. Then, if $i(j)$ is the x coordinate of a point on a chemical distance whose y coordinate is j, $W(l)$ is defined as

$$W(l)=\left[\left\langle \sum_{j=j_0}^{j_0+l}[i(j)-\overline{i}]^2\right\rangle\right]^{1/2}, \tag{5}$$

where angular brackets represent a mean over all portions of length l of the chemical distance and over different realizations of quenched disorder and $\overline{i}$ is the mean horizontal position. For a self-affine path $W(l)\sim l^{\chi}$ holds. In Fig. 7 we show the scaling behavior of $W^2(l)$ versus l for clusters of size $L=128$ and for different values of the parameter η. A

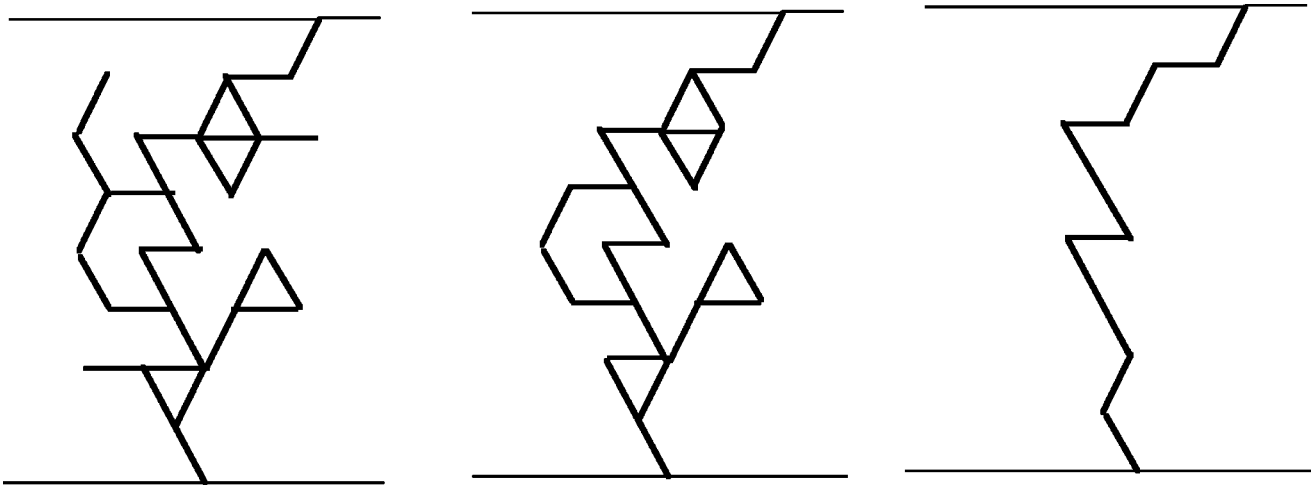

FIG. 4. Schematic representation of an aggregate (left), its backbone (middle), and its chemical distance (right).

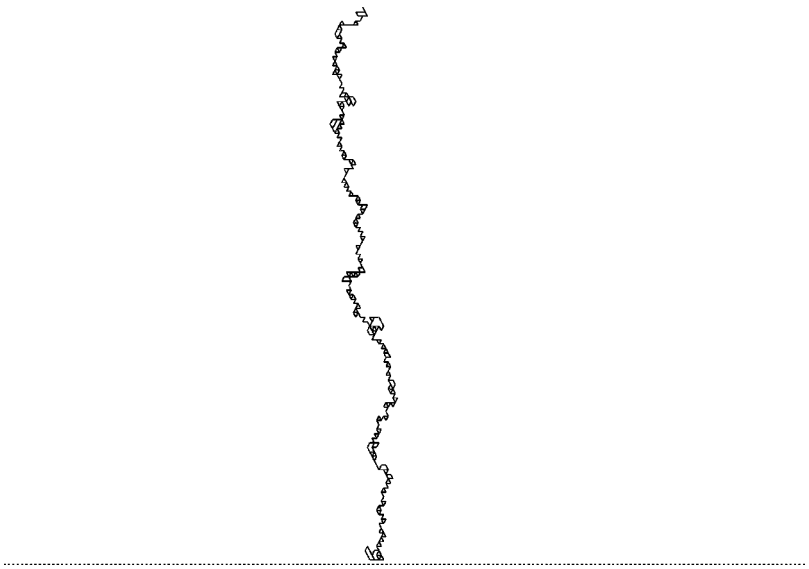

FIG. 5. Backbone of the cluster shown in Fig. 3.

least-squares fit, reported in the figure, gives for values of η ranging over an order of magnitude (from 0.2 to 3) values that seem quite stable within error bars. For $\eta=3$ we get $\chi=0.62\pm0.03$, for $\eta=1.0$ we get $\chi=0.64\pm0.03$, and for $\eta=0.2$ we get $\chi=0.66\pm0.03$.

The independence of χ from η (i.e., from the product $a\,\eta$) indicates a very important universality property of the model. In particular, the values we find are quite similar to that of the directed percolation ($\chi=\nu_{\parallel}/\nu_{\perp}=0.625\ldots$ [19]), so we can suppose that, concerning the chemical distance, the model is in the same universality class of directed percolation.

The evolution of the dynamics towards an asymptotic stationary state is characterized by the acceptance profile $a(x)$. It gives the rate of acceptation (selection by the growth process) for the values of the quenched variables associated with the grown bonds, on the interval $[x,x+dx]$. We have performed a set of ten realizations of size 512×512, for $\eta=1.0,2.0,3.0$, $a=1$ and $\beta=0.5$. This allowed us to follow the time evolution of $a(x)$ up to $t=500$, where the asymptotic state is reached. In Fig. 8 we show the final shape of $a(x)$ for the different values of η. The presence of the stress field prevents the dynamics from developing scale-invariant avalanches and this is reflected in the absence of a critical threshold in $a(x)$ [12]. However, as the value of η becomes smaller and the role of the stress field becomes less relevant, one can see that $a(x)$ seems to develop a discontinuity. What we expect is that in the limit $\eta=0$ one recovers the IP dynamics. Also in this case we obtain results that agree with those obtained for the QDBM [13]. In fact, a common picture, which we describe in a longer paper, can be used to study both models [20].

IV. THEORETICAL RESULTS

In this section we present some theoretical results concerning the universality properties of the model and the explanation of the screening effects that give rise to such fractal breakdown patterns. To demonstrate that all the dynamical and geometrical properties of the model depend only on the product $a\,\eta$ instead of on the two parameters separately, consider the generic variable

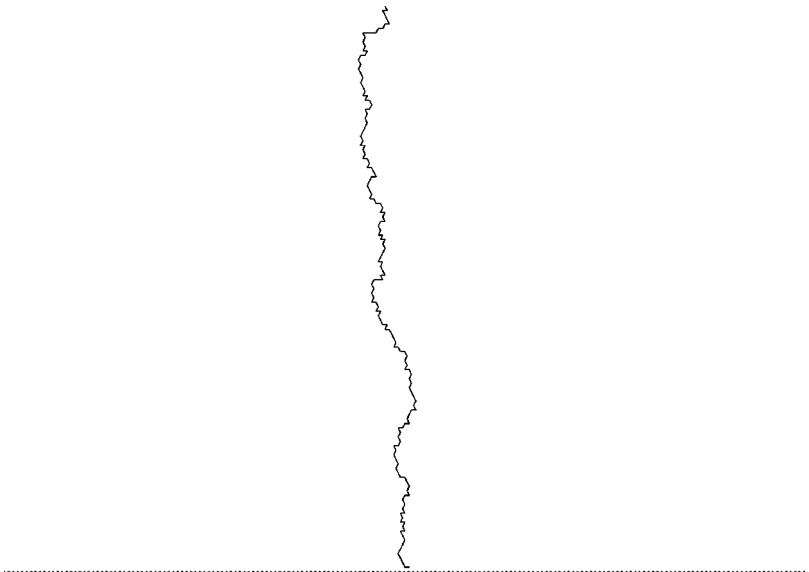

FIG. 6. Chemical distance of the cluster of Fig. 3.

TABLE IV. Behavior of the backbone fractal dimension (D_B) and (D_C) of chemical distance fractal dimension, with $\beta=0.5$, $\alpha=1$, $\eta=1$, and $a=1$, for clusters of size $L=64$ and $L=128$.

L	D_B	D_C
64	1.07 ± 0.02	1.00 ± 0.02
128	1.10 ± 0.02	1.00 ± 0.02

$$y_{i,j}(t)=\frac{x_{i,j}}{V_{i,j}(t)^{\eta/2}}, \tag{6}$$

where $x_{i,j}$ is extracted from the density function

$$p_0(x_{i,j})=\frac{a}{x_{sup}^a}x_{i,j}^{a-1}. \tag{7}$$

Now perform the transformation of the quenched variables

$$z_{i,j}=[x_{i,j}]^a. \tag{8}$$

Introducing Eq. (8) in Eq. (7), one can note that the variables $z_{i,j}$ are uniformly distributed between 0 and $z_{sup}=x_{sup}^a$. So the density function of the new variables will depend on the parameter a only through the value of z_{sup}, which is unique for all variables. Introducing Eq. (8) in Eq. (6), we obtain

$$y_{i,j}(t)=\left[\frac{z_{i,j}}{V_{i,j}(t)^{(a\eta)/2}}\right]^{1/a}. \tag{9}$$

Finally, as the dynamics is extremal it does not change if instead of the variables $y_{i,j}(t)$ we consider as bond variables

$$u_{i,j}(t)=[y_{i,j}(t)]^a=\frac{z_{i,j}}{V_{i,j}(t)^{(a\eta)/2}}. \tag{10}$$

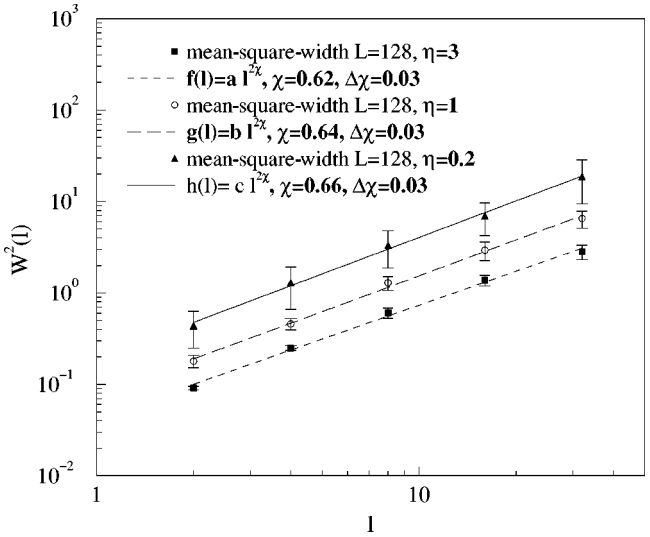

FIG. 7. Scaling behavior of the square mean horizontal width $W^2(l)$ of the chemical distance for clusters of size $L=128$ and different values of η.

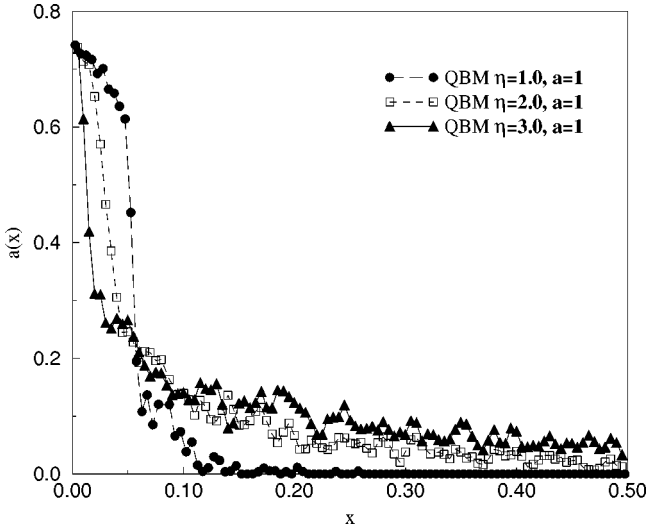

FIG. 8. Acceptation profiles for the variables x_i associated with the grown bonds, for different values of η, after $t=500$ time steps. The absence of a threshold value for $a(x)$ implies a smooth growth (not by avalanches). Moreover, one can note a dependence on the value of η, suggesting that in the limit $\eta=0$ we recover the IP dynamics with a threshold.

This equation shows that all the dynamical and geometrical properties of the model depend only on the product $a\eta$, as asserted before.

Now we switch to the explanation of how the two screening effects (the geometrical one and the probabilistic one) cooperate in the model during the dynamical evolution. In doing so we will briefly introduce a generalized version of the run time Statistics (RTS), which was introduced to study extremal dynamics in quenched disordered media, such as IP [14,12]. The RTS approach consists in a transformation of the deterministic quenched extremal dynamics in a stochastic one through the introduction of effective, time-dependent, density functions for the dynamical variables $y_{i,j}$. The role of these densities is to store information on the past growth history of the system [12,14]. This approach allows us to have a well-defined growth probability distribution at any time step and an updating rule of the effective density functions after any elementary growth event.

To explain simply the observed screening effects, suppose there are only two bonds 1 and 2 in the interface at time t_0 and consider $a=1$ and $\eta>0$. Let the quenched variables of the two bonds be, respectively, x_1 and x_2, which are uniformly distributed between 0 and 1. Moreover, let the related stress fields be, respectively, $E_{1,t_0}=V_1(t)^{\eta/2}$ and $E_{2,t_0}=V_2(t)^{\eta/2}$, where, for example, without loss of generality, $E_{1,t_0}\geqslant E_{2,t_0}$. Then we have $y_{i,t_0}=x_i/E_{i,t_0}$ for $i=1,2$ uniformly distributed between 0 and $1/E_{i,t_0}$, i.e.,

$$p_{i,t_0}(y)=E_{i,t_0} \quad i=1,2. \tag{11}$$

$p_{i,t_0}(y)$ represents the effective density of the bond i at time t_0. We want now to calculate the probability μ_{1,t_0} that bond 1 grows at t_0+1, i.e., that $y_{1,t_0}<y_{2,t_0}$. This probability is given by

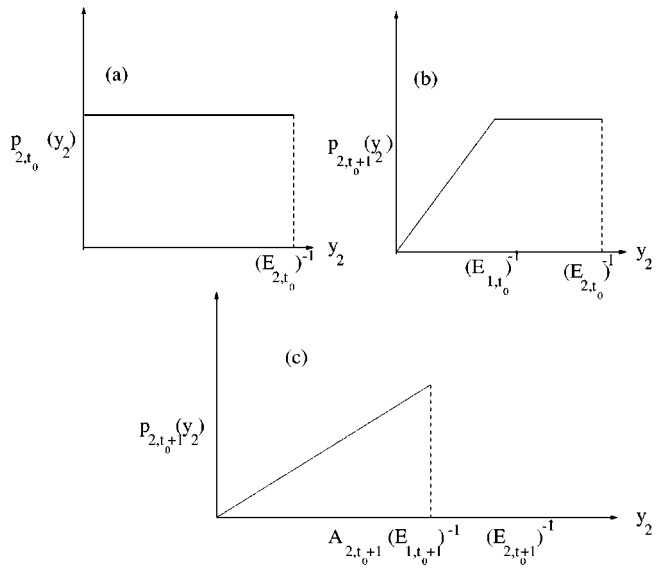

FIG. 9. (a) Density function of bond 2 at time t_0 and (b) density function $p_{2,t_0+1}(y_2)$ of bond 2 at time t_0+1, under the hypothesis of constant stress field. This density concentrates more on high values. (c) If one adds the geometric screening of the stress field, the $p_{2,t_0+1}(y_2)$ concentrates even more on higher values, reflecting the cooperation of the two kinds of screening.

$$\mu_{1,t_0}=\int_0^{1/E_{1,t_0}} dy_1 E_{1,t_0}\int_{y_1}^{1/E_{2,t_0}} dy_2 E_{2,t_0}=1-\frac{E_{2,t_0}}{2E_{1,t_0}}\geqslant\frac{1}{2}. \tag{12}$$

Now we suppose that this is the real growth event and compute the new probability density $p_{2,t_0+1}(y_2)$ of the variable y_{2,t_0+1} conditioned to that event. For the sake of simplicity, we assume that the stress field of bond 2 remains constant, i.e., $y_{2,t_0+1}=y_{2,t_0}$. By applying the rules of conditional probability, we obtain

$$p_{2,t_0+1}(y_2)=p_{2,t_0}(y_2)\int_0^{y_2} dy_1 p_{1,t_0}(y_1)\,\theta(1/E_{1,t_0}-y_1), \tag{13}$$

where the function θ is the step function and indicates that the variable y_1 must be smaller than $1/E_{1,t_0}$. By introducing Eq. (11) in Eq. (13), we obtain

$$p_{2,t_0+1}(y_2)=\begin{cases}\dfrac{E_{2,t_0}E_{1,t_0}}{\mu_{1,t_0}}y_2, & 0\leqslant y_2\leqslant\dfrac{1}{E_{1,t_0}}\\[2ex] \dfrac{E_{2,t_0}}{\mu_{1,t_0}}, & \dfrac{1}{E_{1,t_0}}\leqslant y_2\leqslant\dfrac{1}{E2,t_0}.\end{cases} \tag{14}$$

This function is represented in Fig. 9(b) and the effective probability density of y_2 at time t_0+1 is more concentrated towards the high values of the variable than at time t_0, at which it was uniform. If we introduce this density in Eq. (12), we see that the growth probability of bond 1 increases and by normalization the growth probability of bond 2 decreases. This is what was called before the probabilistic screening effect, which is nothing but a memory effect. In deriving Eq. (14) we made the hypothesis that the stress field of bond 2 remains constant. In general, this is not the case; in fact, when a bond i grows at time t the stress field of a bond j remaining on the growth-interface decreases, i.e., $E_{j,t+1}\leqslant E_{j,t}$. This leads to the second kind of screening: the geometric one. In fact, supposing $E_{2,t_0+1}\leqslant E_{2,t_0}$, we obtain

$$y_{2,t_0+1}=\frac{E_{2,t_0}}{E_{2,t_0+1}}y_{2,t_0}=A_{2,t_0+1}y_{2,t_0}. \tag{15}$$

Note that, as $A_{2,t_0+1}\leqslant 1$, we have $y_{2,t_0+1}\leqslant y_{2,t_0}$. From Eqs. (14) and (15) we obtain the effective probability density of the dynamical variable of the bond 2:

$$p_{2,t_0+1}(y_2)=\begin{cases}\dfrac{E_{2,t_0+1}E_{1,t_0}}{\mu_{1,t_0}}\dfrac{y_2}{A_{2,t_0+1}}, & 0\leqslant y_2\leqslant\dfrac{A_{2,t_0+1}}{E_{1,t_0}}\\[2ex] \dfrac{E_{2,t_0+1}}{\mu_{1,t_0}}, & \dfrac{A_{2,t_0+1}}{E_{1,t_0}}\leqslant y_2\leqslant\dfrac{1}{E2,t_0+1},\end{cases} \tag{16}$$

where now we account for the decrease of the stress field in the variable y_2. Since, by definition, $A_{2,t_0+1}>1$, this function is more concentrated towards the high values of the variable than in the previous case [Fig. 9(c)]. Thus the growth probability of bond 2 further decreases with respect to Eq. (14). This reflects the presence of both screening effects: the geometric one due to the decreasing stress fields of ''old'' perimeter bonds and the temporal one produced by memory effects. In this way we have shown simply how the two kinds of screening effects add the evolution of the dynamics leading to a fractal structure with small fractal dimensions.

The generalization of these arguments to the case in which the interface is composed of many bonds with different initial probability densities leads to the formulation of the RTS for extremal dynamics with quenched disorder and a driving field, which has been introduced in [13] to study the problem of the electric discharge in disordered dielectric system.

V. CONCLUSIONS

We have introduced and studied a model for the dynamics of fractures in a quenched random medium. The model exhibits interesting properties, for example, a strong reduction of its fractal dimension with respect to the case of a dominating thermal noise (stochastic dynamics [9]) and a roughness exponent for the chemical distance whose value seems to be independent on the model parameters. Moreover, the fractal dimension of the fractures depends continuously on the material properties, represented in the model by a power-law distribution of quenched disorder with a tunable parameter a. This is, from an experimental point of view, reasonable. In a situation in which thermal fluctuations of the lattice are irrelevant, the only source of noise, and thus of fractal properties, in the growth process is the intrinsic quenched disorder of the samples (impurities, vacancies, etc.). Our model, however, is still too idealized to allow a quantitative comparison with experiments.

It would be interesting to compute analytically the fractal

dimension of this model by using the fixed scale transformation (FST) [21] approach, after having mapped its dynamics onto a stochastic one, with the RTS method. The mapping is in fact possible, but the approximations one has to use in the FST approach give rise to quite poor numerical results, as reported in a longer paper on this subject [20].

The model can be further generalized. A research direction we are presently following concerns the unification of the low-temperature (deterministic, extremal dynamics with quenched disorder) and high-temperature (stochastic dynamics with thermal noise) regimes by the introduction of a temperaturelike parameter T that can tune the transition between the two regimes [22]. This could represent a further step toward a more realistic description of fracture propagation in solids. One interesting property of this generalized model is that in the high-temperature limit, the level of approximation of the FST method becomes excellent [21]. This could allow us to get a good estimation of the low-temperature fractal dimension by an extrapolation of the values we get in the high-temperature case.

[1] *Statistical Models for the Fracture of Disordered Media*, edited by H. J. Herrmann and S. Roux (Elsevier, Amsterdam, 1990).
[2] T. Vicsek, *Fractal Growth Phenomena* (World Scientific, Singapore, 1992).
[3] H. J. Herrmann, Phys. Scr. **T38**, 13 (1991).
[4] S. Zapperi, P. Ray, H. E. Stanley, and A. Vespignani, Phys. Rev. Lett. **78**, 1408 (1997).
[5] L. Niemeyer, L. Pietronero, and H. J. Wiessmann, Phys. Rev. Lett. **52**, 1033 (1984).
[6] T. A. Witten and L. M. Sander, Phys. Rev. Lett. **47**, 1400 (1981).
[7] D. Wilkinson and J. F. Willemsen, J. Phys. A **16**, 3365 (1983).
[8] H. Yan, G. Li, and L. M. Sander, Europhys. Lett. **10**, 7 (1989).
[9] G. Caldarelli, C. Castellano, and A. Vespignani, Phys. Rev. E **49**, 2673 (1993).
[10] C. Evertsz, Phys. Rev. A **41**, 1830 (1990).
[11] M. Paczuski, P. Bak, and S. Maslov, Phys. Rev. E **53**, 414 (1996).
[12] R. Cafiero, A. Gabrielli, M. Marsili, and L. Pietronero, Phys. Rev. E **54**, 1406 (1996).
[13] R. Cafiero, A. Gabrielli, M. Marsili, L. Pietronero, and L. Torosantucci, Phys. Rev. Lett. **79**, 1503 (1997).
[14] M. Marsili, J. Stat. Phys. **77**, 733 (1994); A. Gabrielli, M. Marsili, R. Cafiero, and L. Pietronero, *ibid.* **84**, 889 (1996).
[15] E. Louis and F. Guinea, Europhys. Lett. **3**, 871 (1987).
[16] P. Meakin, G. Li, L. M. Sander, E. Louis, and F. Guinea, J. Phys. A **22**, 1393 (1989).
[17] G. Caldarelli, F. Di Tolla, and A. Petri, Phys. Rev. Lett. **77**, 2503 (1996).
[18] K. Sneppen, Phys. Rev. Lett. **69**, 3539 (1992).
[19] See, e.g., the exhaustive review T. Halpin-Healy and Y.-C. Zhang, Phys. Rep. **254**, 215 (1995), and references therein.
[20] A. Gabrielli, R. Cafiero, M. Marsili, L. Pietronero, and L. Torosantucci (unpublished).
[21] A. Erzan, L. Pietronero, and A. Vespignani, Rev. Mod. Phys. **67**, 545 (1995).
[22] R. Cafiero, A. Gabrielli, M. Marsili, M. A. Munoz and L. Pietronero (unpublished).